analytical chemistry

pubs.acs.org/ac Article

K-Doped Graphitic Carbon Nitride with Obvious Less Electrode Passivation for Highly Stable Electrochemiluminescence and Its Sensitive Sensing Analysis of MicroRNA

Linlei Liu, Yusen Liu, Yue Zhang, Ruo Yuan,* and Haijun Wang*

Cite This: *Anal. Chem.* 2022, 94, 7191−7199 Read Online

ACCESS | Metrics & More | Article Recommendations | Supporting Information

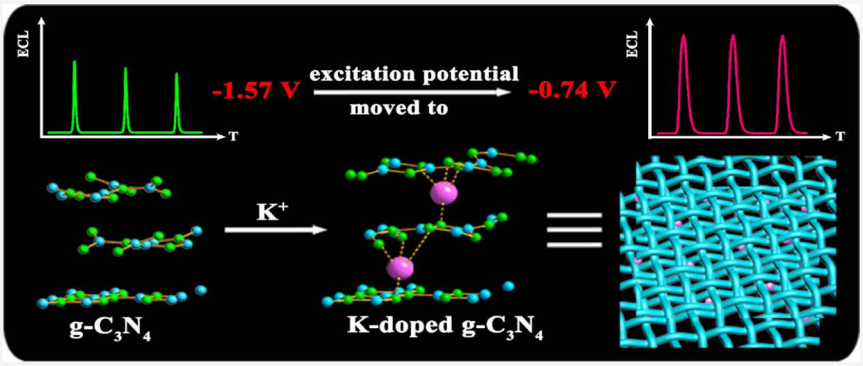

ABSTRACT: In this study, upon potassium (K) element doping, the electrochemiluminescence (ECL) excitation potential of graphitic carbon nitride (g-C_3N_4) obviously shifted from −1.57 to −0.74 V. Compared with other reported methods, this work was the first one that could reduce the ECL excitation potential of g-C_3N_4 to below the critical value of −0.9 V. It could more effectively overcome electrode passivation and significantly improve the ECL intensity and stability. Meanwhile, the lower excitation potential could significantly reduce other side reactions caused by high voltage, and the introduction of the K element could obviously increase the water solubility to shorten the preparation time. The apparent decrease of the excitation potential was due to the doping of the K element, which could reduce the band gap, increase the in-plane spacing, and expand π-conjugated systems. Furthermore, using K-doped g-C_3N_4 with highly stable electrochemiluminescence at lower potential as an emitter, a biosensor for microRNA-141 (miRNA-141) sensitive detection was constructed with the assistance of an innovative nicking enzyme-assisted strand displacement amplification (N-SDA). Compared to the traditional SDA, a nicking enzyme was introduced to obviously improve the utilization rate of the fuel chain and increase the number of cycles, finally resulting in higher signal amplification efficiency. Therefore, the constructed biosensor showed excellent performance in the ultrasensitive detection of miRNA-141 with the limit of detection (LOD) being 44.8 aM. This work gave a more effective means to obviously improve the ECL property of g-C_3N_4 caused by electrode passivation and provided a more efficient and convenient detection method for biochemical analysis.

INTRODUCTION

Graphite-like-phase carbon nitride (g-C_3N_4) is a kind of two-dimensional nonmetallic nanomaterial with simple synthesis, good biocompatibility, easy functionalization, and controllable band gap,[1−5] which is widely used in photocatalysis,[6−8] electrocatalysis,[9−11] pollutant degradation,[12,13] and biosensors[14−19] due to its excellent photoelectric properties and catalytic ability. Since the electrochemiluminescence (ECL) phenomenon of g-C_3N_4 with $K_2S_2O_8$ as a coreactant was first discovered in 2012,[20] it has resulted in an upsurge of research. Chen and co-workers found that g-C_3N_4 exhibited electrode passivation when the ECL excitation voltage exceeded −0.9 V.[21] The main reason was that excited electrons were continuously poured into the conduction bands when the scanning voltage exceeded −0.9 V, which led to partial electrical reduction of g-C_3N_4, weakening of the conductivity, and gradual decrease in the ECL response. In addition, g-C_3N_4 had poor water solubility, which usually required ultrasonic treatment for more than 10 h. These defects seriously limited the better application of g-C_3N_4 in the ECL field.

To solve the above problems, the current research mainly started from the following two aspects. The first solution was the introduction of metal nanoparticles (such as AuNPs,[16,17,21]

Received: December 15, 2021
Accepted: May 4, 2022
Published: May 13, 2022

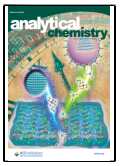

https://doi.org/10.1021/acs.analchem.1c05440
Anal. Chem. 2022, 94, 7191−7199

Scheme 1. Schematic Representation of (A) Structure Model and Synthesis Process of AuNPs@K-doped g-C_3N_4; (B) Electrode Modification Process; (C) Signal Amplification Process of Nicking Enzyme-Assisted Strand Displacement Reaction

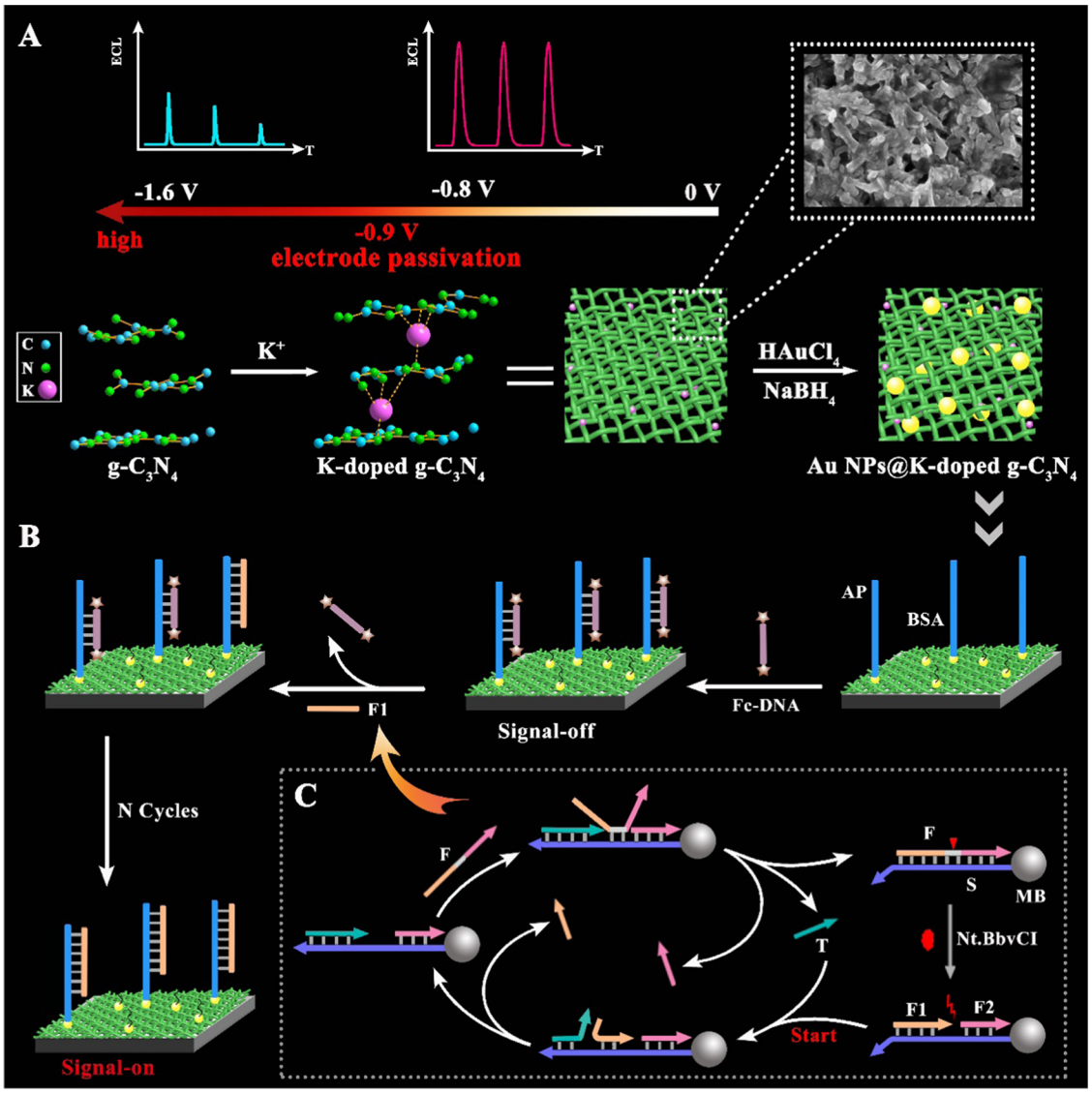

AgNPs,[18] and PtNPs[19]) to mediate the overinjected electrons into the g-C_3N_4 conduction bands by transferring some electrons to metal NPs, among which AuNPs had the most outstanding performance. Chen et al. first proposed that AuNPs could be used to solve this problem after proposing electrode passivation, and its initial potential and excitation potential moved forward by 50 and 90 mV, respectively.[21] Moreover, another solution was the introduction of element vacancies.[22−24] Du et al. introduced oxygen vacancies by doping rare-earth element (Eu^{3+}) into g-C_3N_4 synthesis, which showed a tunable ECL wavelength.[23] The ECL initial potential was shifted positively by 420 mV, and the ECL excitation potential moved from −1.6 to −1.5 V. Subsequently, Zou et al. adjusted the intrinsic electronic structure of g-C_3N_4 by introducing nitrogen vacancies that acted as electron traps, which could accelerate the electron transfer and stored overinjection electrons.[24] Its initial potential and ECL excitation potential shifted forward by 200 and 50 mV, respectively. Although the above methods have improved the stability of g-C_3N_4 to a certain extent, the peak potential of g-C_3N_4 was still greater than −0.9 V, which would still lead to obvious electrode passivation. Meanwhile, the water solubility of g-C_3N_4 was not obviously improved, and it still needed a long time of ultrasonic treatment. Thus, to preferably ameliorate water solubility and reduce electrode passivation for improving the ECL performance of g-C_3N_4, we attempted to explore new means to modulate the band gap by using element doping.

In this study, K-doped g-C_3N_4 with a low cathode ECL excitation potential (−0.74 V) was synthesized, showing excellent stability and an ultrahigh ECL response. As shown in Scheme 1A, the K atom was doped between the lamellae of g-C_3N_4, which could improve the ECL intensity and stability compared to the pristine g-C_3N_4. The introduction of the K atom expanded π-conjugated systems and reduced the band gap, which greatly reduced the ECL excitation potential. And the ECL excitation potential of the proposed K-doped g-C_3N_4 was more positive than −0.9 V, which more effectively avoided electrode passivation compared with previous studies. Meanwhile, the introduction of the K element increased the water solubility of g-C_3N_4, which suggested that K-doped g-C_3N_4 nanosheets with good dispersion and excellent performance

https://doi.org/10.1021/acs.analchem.1c05440
Anal. Chem. 2022, 94, 7191−7199

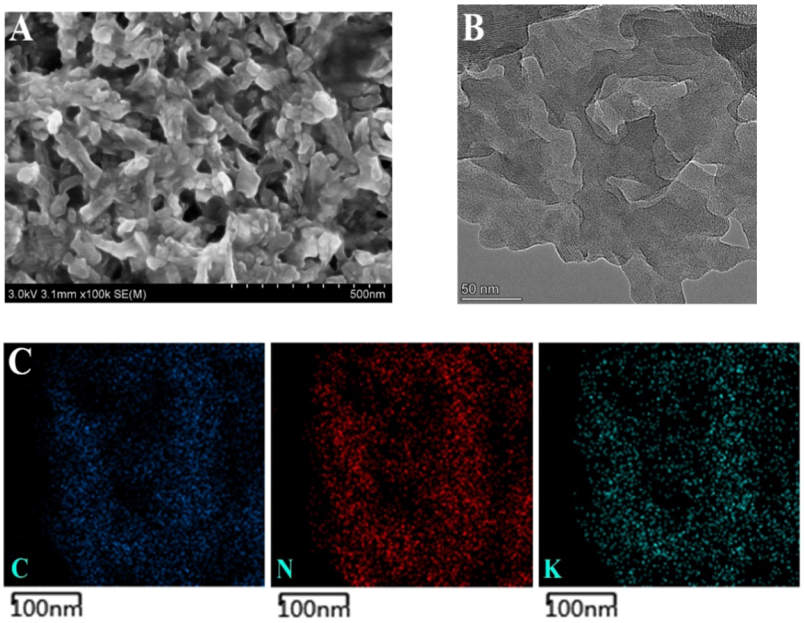

Figure 1. SEM (A) and TEM images (B) and elemental mappings (C) of C, N, and K for the K-doped g-C_3N_4.

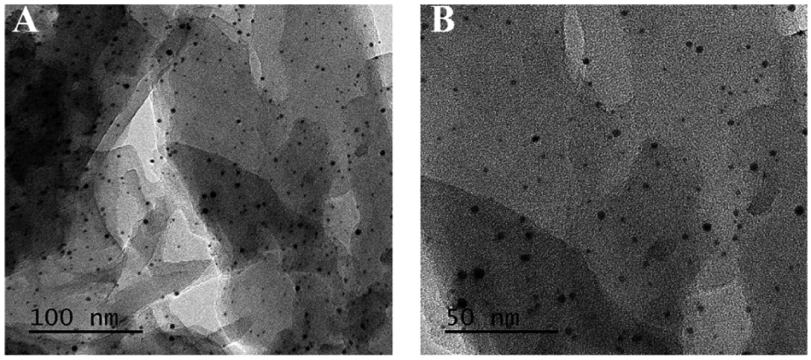

Figure 2. TEM images of AuNPs@K-doped g-C_3N_4 at scale bars of 100 nm (A) and 50 nm (B).

could be obtained only after 3 h of ultrasonic treatment. In addition, the lower excitation voltage could effectively avoid other side reactions caused by high voltage. Then, we further synthesized the AuNPs@K-doped g-C_3N_4 composites by an in situ reduction method. AuNPs could not only facilitate the construction of subsequent sensors but also accelerate the conversion of $S_2O_8^{2-}$ to $SO_4^{\bullet-}$ for promoting the ECL intensity. After that, an ECL biosensor with K-doped g-C_3N_4 as an ECL emitter was constructed to achieve sensitive detection of microRNA-141 (miRNA-141). As shown in Scheme 1C, the signal amplification of the miRNA-141 was realized by nicking enzyme-assisted strand displacement amplification (N-SDA). Compared with the traditional SDA, the introduction of Nt.BbvCI could improve the utilization rate of combustion chain F and increase the number of cycles to improve the signal amplification efficiency. The quenching probe Fc-DNA was modified on the electrode interface to obtain a "signal-off" state. However, Fc-DNA could be removed to achieve a "signal-on" state by introducing output DNA (F1), which realized sensitive detection of miRNA-141.

EXPERIMENTAL SECTION

Synthesis of AuNPs@K-Doped g-C_3N_4. All chemicals were analytical grade and used without further purification. First, g-C_3N_4 was prepared according to refs 7, 25, and the specific steps were as follows: 1.5 g of melamine was placed in a porcelain cup and heated to 550 °C for 4 h in a muffle furnace with the heating rate and cooling rate of 2 and 10 °C/min, respectively. Then, the obtained product was dissolved in water (0.5 mg/mL) and treated with ultrasound for more than 10 h. Second, the preparation process of K-doped g-C_3N_4 was the same as that of g-C_3N_4,[7,25] but 3 mmol of NaOH, 0.08 mol of KCl, and melamine needed to be ground and mixed evenly before calcination. After calcination, the product was washed, centrifuged, and vacuum freeze-dried to obtain pure K-doped g-C_3N_4. In addition, the product only needed ultrasonic treatment for 3 h after being dissolved in water (0.5 g/L) in comparison to g-C_3N_4.

The AuNPs@K-doped g-C_3N_4 was prepared as follows: 10 μL of $HAuCl_4$ (0.01 M) was injected into 1 mL of K-doped g-C_3N_4 solution and stirred for 2 h. After that, 25 μL of fresh $NaBH_4$ solution (0.01 M) was slowly dropped into the above solution and stirred for 20 min. Subsequently, 10 μL of trisodium citrate (0.01 M) was added with stirring for 30 min. Finally, the obtained solution was centrifuged and washed with ultrapure water.

Measurement Procedure. The modified electrode was tested in 2 mL of phosphate-buffered saline (PBS) (pH 7.4)

https://doi.org/10.1021/acs.analchem.1c05440
Anal. Chem. 2022, 94, 7191−7199

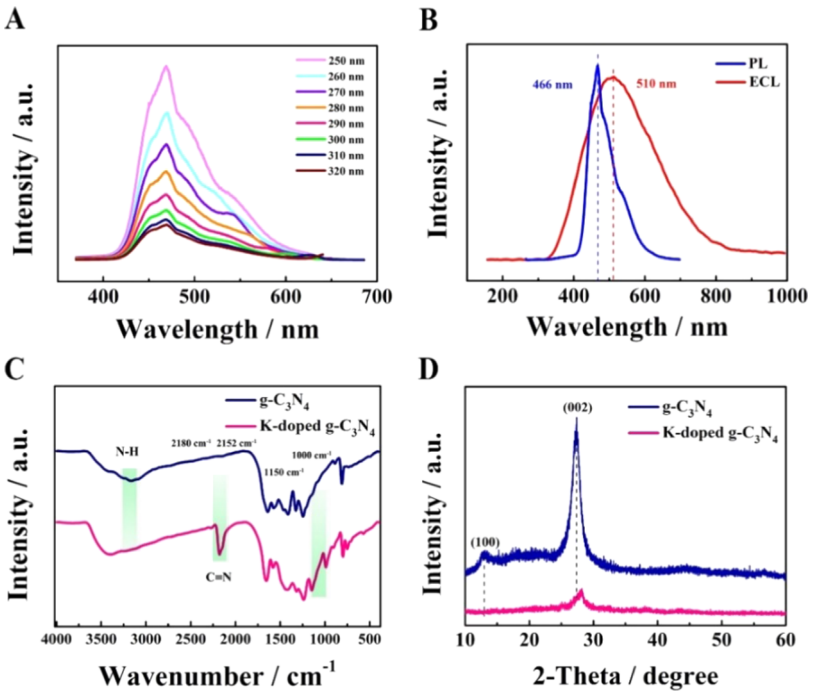

Figure 3. (A) PL emission spectra of K-doped g-C_3N_4 at different excitation wavelengths. (B) PL and ECL spectra of K-doped g-C_3N_4. (C, D) FT-IR and XRD spectra of g-C_3N_4 and K-doped g-C_3N_4.

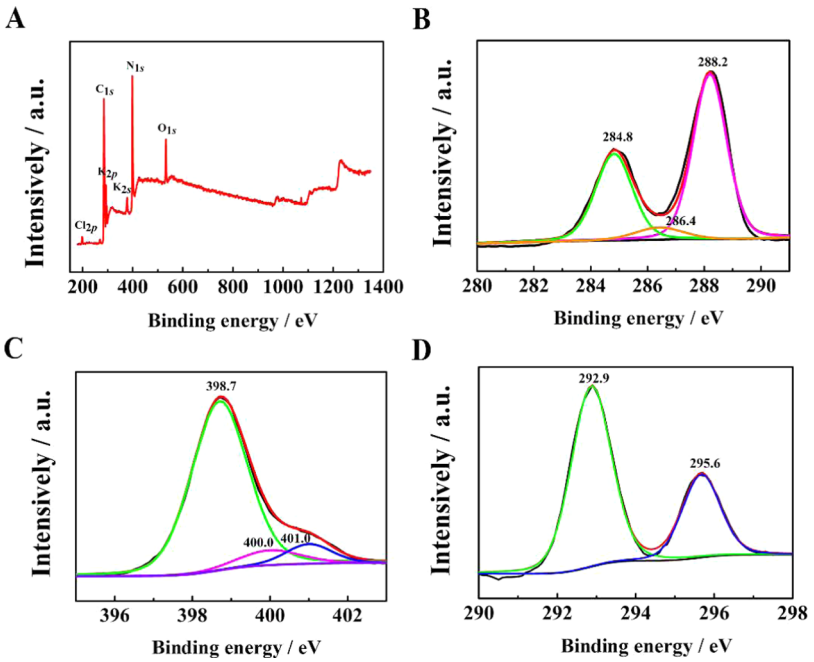

Figure 4. XPS spectra of (A) K-doped g-C_3N_4, (B) C 1s, (C) N 1s, and (D) K 2p.

containing 1 mM $S_2O_8^{2-}$, and the ECL response was studied with a multiphoton ionization (MPI)-ECL analyzer. The ECL scanning potential was ranged from 0 to −0.8 V with a scan rate of 200 mV/s and the photomultiplier tube (PMT) was 800 V.

RESULTS AND DISCUSSION

Morphological Characterization of Different Materials. The structure, composition, and morphology of the K-doped g-C_3N_4 were studied by scanning electron microscopy (SEM) and transmission electron microscopy (TEM). As shown in Figure 1A, K-doped g-C_3N_4 was formed by stacking porous lamellar structures, and TEM was used to further understand the microstructure of K-doped g-C_3N_4. As shown in Figure 1B, K-doped g-C_3N_4 showed a thin multilayer structure, which was consistent with the literature.[7,25] In addition, the element mapping diagram was used to observe the elemental distribution. As shown in Figure 1C, C and N were the main elements, and K was uniformly distributed in g-C_3N_4, which further proved that the K atom was successfully inserted in g-C_3N_4. Moreover, it could be seen from Figure 2 that many AuNPs were equably distributed on the surface of

https://doi.org/10.1021/acs.analchem.1c05440
Anal. Chem. 2022, 94, 7191−7199

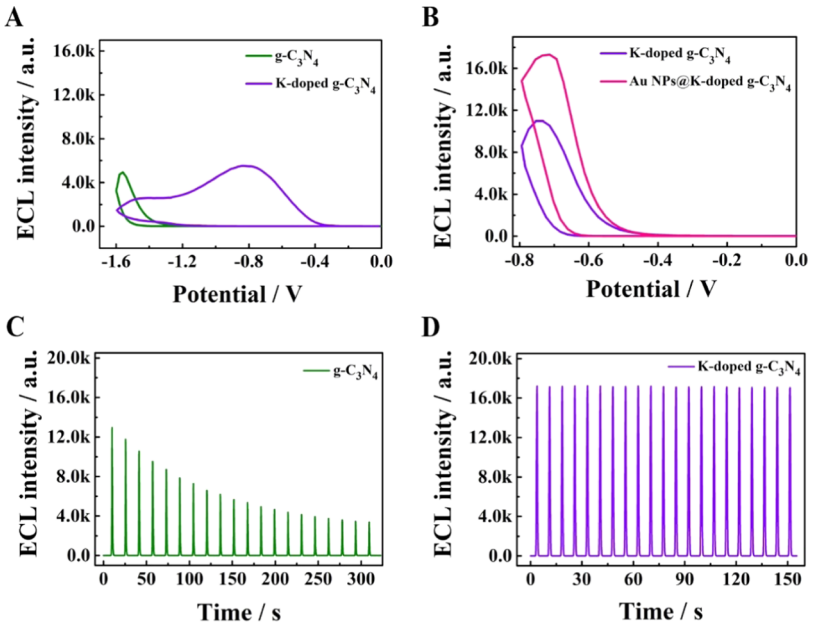

Figure 5. (A) ECL curves of g-C_3N_4 and K-doped g-C_3N_4 from 0 to −1.6 V. (B) ECL curves of K-doped g-C_3N_4 and AuNPs@K-doped g-C_3N_4 from 0 to −0.8 V. The ECL stability of g-C_3N_4 (C) and K-doped g-C_3N_4 (D).

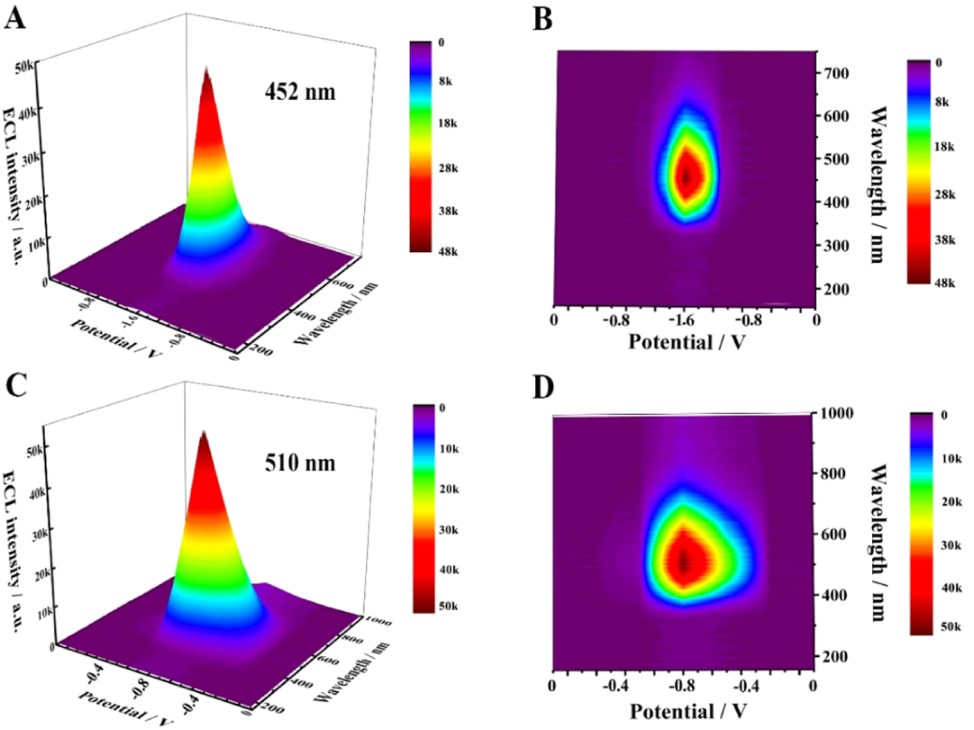

Figure 6. ECL spectra of g-C_3N_4 (A, B) and K-doped g-C_3N_4 (C, D) through three-dimensional (3D) surface imaging and heat map imaging in a 1 mM $S_2O_8^{2-}$ solution.

K-doped g-C_3N_4 nanomaterial, proving that the AuNPs@K-doped g-C_3N_4 was successfully synthesized.

Spectral Characterization of the K-doped g-C_3N_4. To analyze the structure of K-doped g-C_3N_4, the photoluminescence (PL) spectrum, ECL spectrum, Fourier transform infrared (FT-IR) spectra, X-ray diffraction (XRD) patterns, and X-ray photoelectron spectroscopy (XPS) spectra were obtained. As shown in the PL spectra in Figure 3A, the K-doped g-C_3N_4 exhibited emission behavior independent of excitation as the excitation wavelength changed. As seen in Figure 3B, the PL emission wavelength of K-doped g-C_3N_4 was at 466 nm and the ECL emission wavelength was red-shifted to 510 nm, which demonstrated that the change in the surface state played a dominant role in the ECL process.[27] As seen from the FT-IR spectra in Figure 3C, the bands located at 3310 cm^{-1} correspond to the stretching vibration of N−H, and a new absorption band of K-doped g-C_3N_4 appeared at about 2180 cm^{-1}, which was caused by the conversion of −C−NH_2 to the cyano groups (−C≡N). As shown in the XRD spectra in Figure 3D, g-C_3N_4 had two characteristic peaks at 13.0 and

https://doi.org/10.1021/acs.analchem.1c05440
Anal. Chem. 2022, 94, 7191−7199

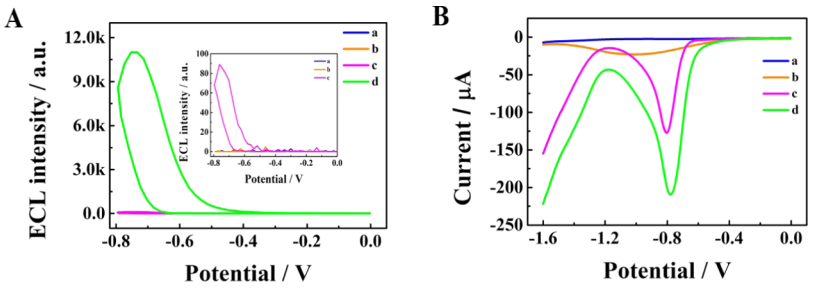

Figure 7. (A) ECL curves and (B) DPV curves of different electrodes of bare GCE (a) and K-doped g-C_3N_4/GCE (c) in PBS and bare GCE (b) and K-doped g-C_3N_4/GCE (d) in PBS containing $S_2O_8^{2-}$.

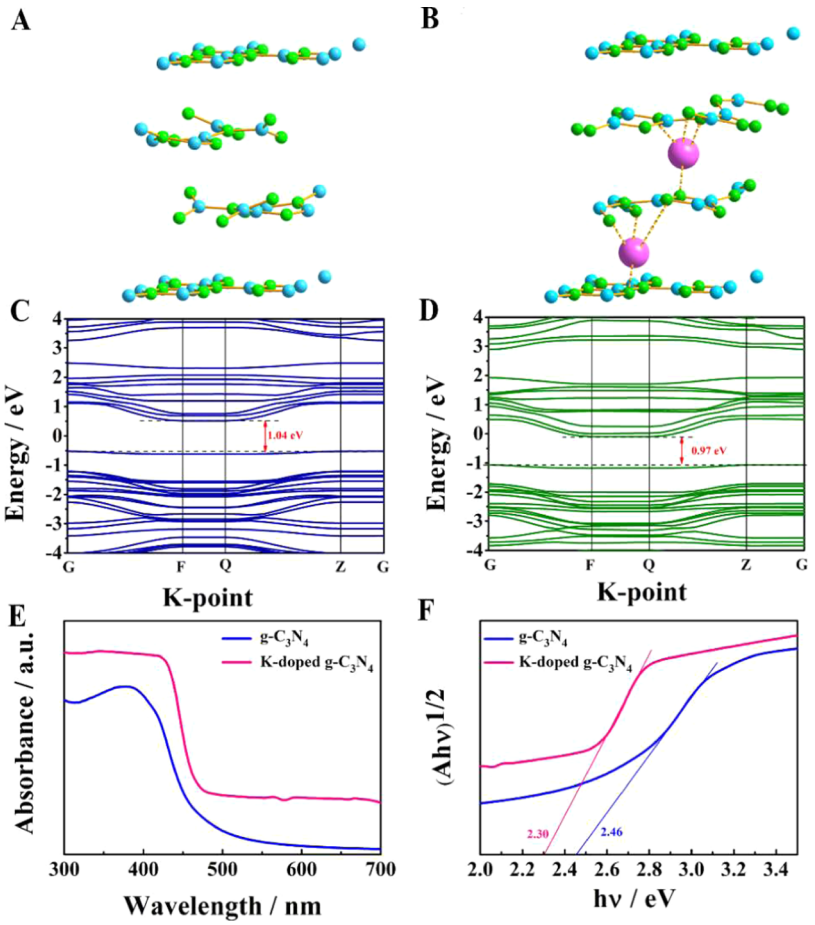

Figure 8. Calculated crystal models and calculated band structure of pure g-C_3N_4 (A, C) and K-doped g-C_3N_4 (B, D). UV−vis diffuse reflectance spectroscopy (E) and band gap (F) of g-C_3N_4 and K-doped g-C_3N_4.

27.4°, corresponding to the (100) and (002) planes, and they represented the in-plane packing and interlayer packing of g-C_3N_4, respectively.[7,25] However, the (100) peak disappeared and the (002) peak shifted upon introducing K into g-C_3N_4 compared with g-C_3N_4, which indicated that K interaction existed in the in-plane and interlayer of K-doped g-C_3N_4.

XPS was used to characterize the bonding state of C, N, and K in K-doped g-C_3N_4. As seen in Figure 4A, the presence of the K 2p peak proved that K was successfully inserted into g-C_3N_4, and the presence of the O 1s peak might be caused by the adsorption of H_2O or O_2 on K-doped g-C_3N_4, which was all consistent with literature reports.[3−5] In the C 1s spectrum, the peaks at 284.8, 288.2, and 286.4 eV corresponded to C−C/C═C bonds, N−C═N bonds, and C−NH_x (x = 1, 2), respectively. As seen in Figure 4C, the N 1s spectrum of K-doped g-C_3N_4 showed three main peaks at 401.0, 400.0, and 398.7 eV, which correspond to NH_x groups, tricoordinated (N_{3C}) nitrogen atoms, and bicoordinated (N_{2C}) nitrogen atoms, respectively. The binding energy of K $2p_{3/2}$ was at 292.9 eV and the peak location of K $2p_{1/2}$ was at 295.6 eV, which corresponded to the interaction of K^+ ions with the surrounding N atom and C atom, respectively.[7] All of the above data indicated that the K-doped g-C_3N_4 was successfully synthesized.

ECL Performance of g-C_3N_4 and K-Doped g-C_3N_4. The ECL performance of g-C_3N_4 and K-doped g-C_3N_4 was compared with regard to ECL excitation potential, stability, and ECL spectrum. First, to compare the influence of K doping on the excitation potential, ECL measurements of g-C_3N_4 and K-doped g-C_3N_4 were performed under the scanning potential

https://doi.org/10.1021/acs.analchem.1c05440
Anal. Chem. 2022, 94, 7191−7199

from 0 to −1.6 V, as shown in Figure 5A. Compared with g-C_3N_4, the peak potential of K-doped g-C_3N_4 was about −0.8 V, indicating that K-doped g-C_3N_4 had more positive cathode ECL excitation potential, which could significantly reduce the influence of electrode passivation. Meanwhile, as shown in Figure 5C,D, the ECL intensity of g-C_3N_4 was unstable due to electrode passivation, but K-doped g-C_3N_4 had more excellent stability. All of the above findings show that introducing K into g-C_3N_4 could reduce electrode passivation by decreasing ECL excitation potential and improving conductivity. In addition, we also explored the influence of AuNPs on K-doped g-C_3N_4. As shown in Figure 5B, AuNPs could obviously boost the ECL intensity of K-doped g-C_3N_4 but not affect the ECL excitation potential.

As shown in the ECL spectra of the 3D surface image (Figure 6A) and heat map image (Figure 6B), there was maximum ECL emission of g-C_3N_4 at 452 nm during the potential between 0 and −1.6 V. However, the maximum ECL emission of K-doped g-C_3N_4 was red-shifted to 510 nm, as shown in Figure 6C,D, which might be due to the decrease in the band gap and expanded π-conjugated systems after K doping.

Possible ECL Mechanism of K-Doped g-C_3N_4. To explore the ECL mechanism of K-doped g-C_3N_4, the ECL response and differential pulse voltammetry (DPV) at different electrodes were measured, as shown in Figure 7. Unmodified GCE had almost no ECL response in PBS with or without $S_2O_8^{2-}$ (Figure 7A, curve a and curve b), and the reduction peak at −1.0 V corresponded to the reduction of $S_2O_8^{2-}$ to $SO_4^{\bullet-}$ (Figure 7B, curve b) (eq 1). Compared with bare GCE, the DPV of K-doped g-C_3N_4/GCE showed the reductive process in PBS with the initial potential around −0.60 V and the maximum response around −0.8 V (Figure 7B, curve c), which indicated that K-doped g-C_3N_4/GCE was electrochemically active through injecting electrons into the lowest unoccupied molecular orbital (LUMO) (eq 2). As shown in curve d of Figure 7B, the reduction current of K-doped g-C_3N_4/GCE was obviously enhanced as $S_2O_8^{2-}$ was introduced. Moreover, K-doped g-C_3N_4/GCE revealed an excellent ECL response in the PBS containing $S_2O_8^{2-}$ compared with that in the PBS without $S_2O_8^{2-}$ (Figure 7A, curve d) (eqs 3 and 4). This result suggested that this strong ECL emission originated from the promotion between $S_2O_8^{2-}$ and K-doped g-C_3N_4. Referring to previous work,[16,21] the possible ECL mechanism was explained as follows

$$S_2O_8^{2-} + e^- \rightarrow SO_4^{\bullet-} + SO_4^{2-} \quad (1)$$

$$\text{K-doped g-}C_3N_4 + e^- \rightarrow \text{K-doped g-}C_3N_4^{\bullet-} \quad (2)$$

$$SO_4^{\bullet-} + \text{K-doped g-}C_3N_4^{\bullet-} \rightarrow SO_4^{2-} + \text{K-doped g-}C_3N_4^{*} \quad (3)$$

$$\text{K-doped g-}C_3N_4^{*} \rightarrow \text{K-doped g-}C_3N_4 + h\nu \quad (4)$$

Effect of K Atom Doping on Band Gap. According to the reported literature,[28−30] the change in the band gap energy would lead to the changes in the ECL excitation potential. Thus, to explore the nature of ECL luminescence potential change after doping K atom, density functional theory (DFT) calculations and the Kubelka−Munk method were performed. On comparing Figure 8A, it could be seen from Figure 8B that the K atom was doped between the lamellae of g-C_3N_4, matching with the XRD data and FT-IR spectra. And this could increase the plane spacing, effectively accelerating the electron transfer. Then, as shown in Figure 8C,D, the energy band structure before and after K atom doping was calculated according to the calculated crystal models, and the band gap changed from 1.04 to 0.97 eV. The doping of the K atom not only changed the in-plane spacing but also reduced the band gap, which directly led to a positive shift of the ECL excitation potential. The ultraviolet diffuse reflectance absorption diagram in Figure 8E indicates that the absorption peak was red-shifted after K atom doping, which is consistent with the reported literature.[7,26] To further understand the influence of K atom, the Kubelka−Munk method[7,25] was used to calculate the band gaps, and the band gap energy of g-C_3N_4 and K-doped g-C_3N_4 were 2.46 and 2.30 eV, which also indicated that doping of the K atom led to the reduction of the band gap. The above data showed that the energy required for excitation decreased because of the decrease of the band gap, which led to the positive shift of the ECL excitation potential.

Feasibility of Nicking Enzyme-Assisted Strand Displacement Amplification. The polyacrylamide gel electrophoresis (PAGE) was used to effectively analyze the feasibility of nicking enzyme-assisted strand displacement amplification. As seen in Figure 9, lanes 1−5 corresponded to the single-stranded DNA of S, F, F1, F2, and target miRNA-141, respectively. A new band at the above position of S, F1, and F2 appeared in lane 6 (S + F1 + F2), indicating the formation of the [S:F1:F2] triple chain structure. After adding miRNA-141 to the [S:F1:F2] triple chain structure, lane 7 exhibited four distinct bands corresponding to the [S:F1:F2] triple chain structure, [S:miRNA-141:F2], F1, and F2. As shown in lane 8, the F2 and miRNA-141 could be liberated through strand displacement when excessive F reacted with the [S:miRNA-141:F2] structure. However, As shown in lane 9, the band corresponding to F disappeared and the band corresponding to F1 and F2 brightened when the Nt.BbvCI was present, proving that the nicking enzyme-assisted strand displacement amplification strategy was successfully realized.

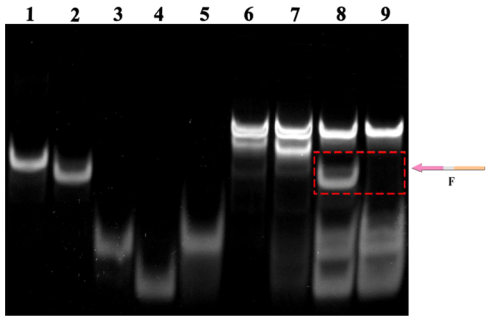

Figure 9. PAGE analysis: lane 1, S; lane 2, F; lane 3, F1; lane 4, F2; lane 5, miRNA-141; lane 6, S + F1 + F2; lane 7, S + F1 + F2 + miRNA-141; lane 8, S + F1 + F2 + miRNA-141 + F; and lane 9, S + F1 + F2 + miRNA-141 + F + Nt.BbvCI.

To prove the superiority of this strategy, we also compared ECL signals of the biosensor with Nt.BbvCI and without Nt.BbvCI (as shown in Figure S7). The ECL response of the biosensor with Nt.BbvCI assistant SDA was about twice that without Nt.BbvCI introduction, which also proved that the nicking enzyme-assisted strand displacement amplification strategy was feasible.

Performance of the Biosensor for miRNA-141 Analysis. First, to prove the successful construction of this

https://doi.org/10.1021/acs.analchem.1c05440
Anal. Chem. 2022, 94, 7191−7199

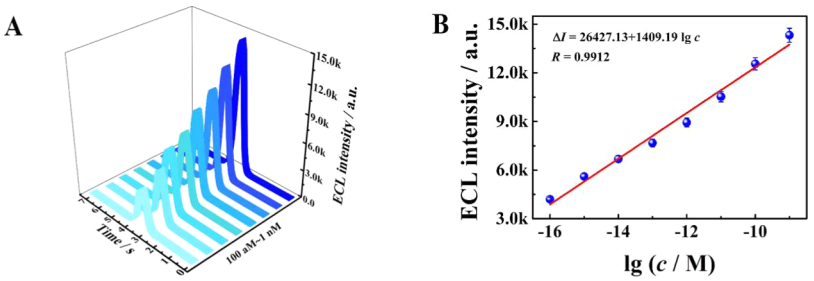

Figure 10. (A) ECL curve of biosensor for different miRNA-141 concentrations. (B) Calibration curve for miRNA-141 analysis.

biosensor, we characterized the construction process of the biosensor by ECL, cyclic voltammetry (CV), and electrochemical impedance spectroscopy (EIS), as shown in Figures S2 and S3. Second, to evaluate the constructed biosensor, the ECL intensity for different concentrations of the target was tested under the optimized conditions (as seen in Figure S6). As seen in Figure 10A, the ECL response increased as the concentration of miRNA-141 increased. As seen in Figure 10B, the ΔI presented a favorable linear response with the logarithm of miRNA-141 changing from 100 aM to 1 nM, and the corresponding regression equation was $\Delta I = 26427.13 + 1409.19 \lg c$ ($R = 0.9912$) with the limit of detection (LOD) for miRNA-141 of 44.8 aM. In addition, as shown in Table S2, this work had a wider response range and lower detection limit, which doubtlessly showed that the detection method of this work had a better application prospect.

Then, the other performances of the constructed biosensor were investigated to evaluate biosensor performance, as shown in the Supporting Information. As shown in Figure S8A, the ECL response had no obvious fluctuation when the number of consecutive scans reached 20, and the relative standard deviation was 2.65%. Subsequently, selectivity was studied by comparing different miRNAs, including miRNA-126, miRNA-182-5p, miRNA-21, and their mixtures containing miRNA-141. As seen in Figure S8B, the ECL response of the mixture containing miRNA-141 was equivalent to that of miRNA-141, which was far higher than that of other miRNA. Meanwhile, the ECL intensity corresponding to miRNA-126, miRNA-182-5p, and miRNA-21 was as low as that of the blank control group. The above data indicated that the constructed biosensor showed good stability and excellent selectivity.

CONCLUSIONS

In summary, K-doped g-C_3N_4 with an ultralow ECL cathode excitation potential was synthesized and applied as a ECL emitter for constructing a biosensor of miRNA-141 sensitive detection. Compared with g-C_3N_4, the interlayer spacing of K-doped g-C_3N_4 was increased and the band gap value was reduced, which led to the ECL excitation potential positively moving from −1.57 to −0.74 V. The ECL excitation potential of the conventional g-C_3N_4 or g-C_3N_4 adjusted by other methods was far negative than −0.9 V; K-doped g-C_3N_4 with low cathode ECL excitation potential in this study could not only effectively avoid electrode passivation effect and improve water solubility but also greatly reduce the side reactions in the ECL reaction process. Then, a nicking enzyme-assisted strand displacement (N-SDA) reaction was adopted to realize the cycle amplification. Compared with the traditional SDA, the novel N-SDA increased the number of cyclic amplification, obviously improving the efficiency of signal amplification by introducing a nicking enzyme. The constructed biosensor had been successfully applied for the sensitive detection of miRNA-141. This study offered a more useful means to reduce electrode passivation of g-C_3N_4 and provided a simple and novel signal amplification way to successfully construct the sensitive biosensor.

ASSOCIATED CONTENT

Supporting Information

The Supporting Information is available free of charge at https://pubs.acs.org/doi/10.1021/acs.analchem.1c05440.

Reagents and materials; instruments; nicking enzyme-assisted strategy to implement target cycling amplification; fabrication of a biosensor; the atomic force microscopy (AFM) characterization of K-doped g-C_3N_4; characterization of the biosensor construction process; the ECL intensity−potential curve of g-C_3N_4 and K-doped g-C_3N_4; EIS of g-C_3N_4 and K-doped g-C_3N_4; optimization of reaction conditions of the biosensor; comparison of the N-SDA with conventional SDA; ECL stability and selectivity of the biosensor; and calculation of the LOD and application (PDF)

AUTHOR INFORMATION

Corresponding Authors

Ruo Yuan − *Key Laboratory of Luminescence Analysis and Molecular Sensing (Southwest University), Ministry of Education, College of Chemistry and Chemical Engineering, Southwest University, Chongqing 400715, People's Republic of China;* orcid.org/0000-0003-3664-6236; Phone: +86-23-68252277; Email: yuanruo@swu.edu.cn; Fax: +86-23-68253172

Haijun Wang − *Key Laboratory of Luminescence Analysis and Molecular Sensing (Southwest University), Ministry of Education, College of Chemistry and Chemical Engineering, Southwest University, Chongqing 400715, People's Republic of China;* orcid.org/0000-0002-6629-8407; Email: hjwang@swu.edu.cn

Authors

Linlei Liu − *Key Laboratory of Luminescence Analysis and Molecular Sensing (Southwest University), Ministry of Education, College of Chemistry and Chemical Engineering, Southwest University, Chongqing 400715, People's Republic of China*

Yusen Liu − *Key Laboratory of Luminescence Analysis and Molecular Sensing (Southwest University), Ministry of Education, College of Chemistry and Chemical Engineering, Southwest University, Chongqing 400715, People's Republic of China*

https://doi.org/10.1021/acs.analchem.1c05440
Anal. Chem. 2022, 94, 7191−7199

Yue Zhang − *Key Laboratory of Luminescence Analysis and Molecular Sensing (Southwest University), Ministry of Education, College of Chemistry and Chemical Engineering, Southwest University, Chongqing 400715, People's Republic of China*

Complete contact information is available at: https://pubs.acs.org/10.1021/acs.analchem.1c05440

Notes

The authors declare no competing financial interest.

■ ACKNOWLEDGMENTS

This work was financially supported by the National Natural Science Foundation (NNSF) of China (21804110), the Natural Science Foundation Project of CQ CSTC (cstc2020jcyj-msxmX0277), and the Venture & Innovation Support Program for Chongqing Overseas Returnees (cx2019059, cx2020015).

■ REFERENCES

(1) Zhou, X.; Liu, Y. R.; Jin, Z. Y.; Huang, M. N.; Zhou, F. F.; Song, J.; Qu, J. L.; Zeng, Y. J.; Qian, P. C.; Wong, W. Y. *Adv. Sci.* **2021**, *8*, 2002456−2002473.
(2) Zhao, T. T.; Zhou, Q.; Lv, Y. Q.; Han, D.; Wu, K. Q.; Zhao, L. F.; Shen, Y. F.; Liu, S. Q.; Zhang, Y. J. *Angew. Chem., Int. Ed.* **2020**, *59*, 1139−1143.
(3) Bai, L. Q.; Huang, H. W.; Zhang, S. G.; Hao, L.; Zhang, Z.; Li, H. F.; Sun, L.; Guo, L.; Huang, H.; Zhang, Y. H. *Adv. Sci.* **2020**, *7*, 2001939−2001947.
(4) Lv, Y. Q.; Zhou, Z. X.; Shen, Y. F.; Zhou, Q.; Ji, J. J.; Liu, S. Q.; Zhang, Y. J. *Sens. Actuators, B* **2018**, *3*, 1362−1367.
(5) Peng, G. M.; Xing, L. D.; Barrio, J.; Volokh, M.; Shalom, M. *Angew. Chem., Int. Ed.* **2018**, *57*, 1186−1192.
(6) Xia, P. F.; Antonietti, M.; Zhu, B. C.; Heil, T.; Yu, J. G.; Cao, S. W. *Adv. Funct. Mater.* **2019**, *29*, 1900093−1900101.
(7) Zhang, P.; Sun, D. G.; Cho, A.; Weon, S.; Lee, S.; Lee, J.; Han, J. W.; Kim, D. P.; Choi, W. *Nat. Commun.* **2019**, *10*, No. 940.
(8) Cheng, L.; Zhang, H. W.; Li, X.; Fan, J. J.; Xiang, Q. J. *Small* **2021**, *17*, 2005231−2005252.
(9) Han, X. P.; Zhang, W.; Ma, X. Y.; Zhong, C.; Zhao, N. Q.; Hu, W. B.; Deng, Y. D. *Adv. Mater.* **2019**, *31*, 1808281−1808290.
(10) Chu, K.; Li, Q. Q.; Liu, Y. P.; Wang, J.; Cheng, Y. H. *Appl. Catal., B* **2020**, *267*, 118693−118700.
(11) Yu, H. J.; Shang, L.; Bian, T.; Shi, R.; Waterhouse, G. I. N.; Zhao, Y. F.; Zhou, C.; Wu, L. Z.; Tung, C. H.; Zhang, T. R. *Adv. Mater.* **2016**, *28*, 5080−5086.
(12) Wang, C. C.; Yi, X. H.; Wang, P. *Appl. Catal., B* **2019**, *247*, 24−48.
(13) Chuaicham, C.; Sekar, K.; Xiong, Y. H.; Balakumar, V.; Mittraphab, Y.; Shimizu, K.; Ohtani, B.; Dabo, I.; Sasaki, K. *Chem. Eng. J.* **2021**, *425*, 130502−130513.
(14) Wang, J.; Haghighatbin, M. A.; Shen, W.; Mi, L.; Cui, H. *Anal. Chem.* **2020**, *92*, 7062−7070.
(15) Zou, R.; Teng, X.; Lin, Y. J.; Lu, C. *TrAC, Trends Anal. Chem.* **2020**, *132*, 116054−16069.
(16) Lv, H. Y.; Chen, A. Y.; Cheng, W. Q.; Kong, L. S.; Zhao, M.; Ding, S. J.; Ju, H. X.; Cheng, W. *Anal. Chem.* **2020**, *92*, 15624−15631.
(17) Wang, F. F.; Liu, Y. Q.; Fu, C. P.; Li, N.; Du, M.; Zhang, L. N.; Ge, S. G.; Yu, J. H. *Anal. Chem.* **2021**, *93*, 1702−1708.
(18) Li, X. J.; Guo, Z. K.; Li, J. X.; Zhang, Y.; Ma, H. M.; Pang, X. H.; Du, B.; Wei, Q. *Anal. Chim. Acta* **2015**, *854*, 40−46.
(19) Mo, G. C.; He, X. M.; Qin, D. M.; Meng, S.; Wu, Y. S.; Deng, B. Y. *Biosens. Bioelectron.* **2021**, *178*, 113024−113031.
(20) Cheng, C. G.; Huang, Y.; Tian, X. Q.; Zheng, B. Z.; Li, Y.; Yuan, H. Y.; Xiao, D.; Xie, S. P.; Choi, M. M. F. *Anal. Chem.* **2012**, *84*, 4754−4759.
(21) Chen, L. C.; Zeng, X. T.; Si, P.; Chen, Y. M.; Chi, Y. W.; Kim, D. H.; Chen, G. N. *Anal. Chem.* **2014**, *86*, 4188−4195.
(22) Zou, R.; Xie, R. Y.; Wang, L. R.; Lin, Y. J.; Lu, C. *Chem. Commun.* **2022**, *58*, 423−426.
(23) Du, X. J.; Jiang, D.; Dai, L. M.; Zhu, W. R.; Yang, X. D.; Hao, N.; Wang, K. *Anal. Chem.* **2018**, *90*, 3615−3620.
(24) Zou, R.; Lin, Y. J.; Lu, C. *Anal. Chem.* **2021**, *93*, 2678−2686.
(25) Yu, H. J.; Shi, R.; Zhao, Y. X.; Bian, T.; Zhao, Y. F.; Zhou, C.; Waterhouse, G. I. N.; Wu, L. Z.; Tung, C. H.; Zhang, T. R. *Adv. Mater.* **2017**, *29*, 1605148−1605154.
(26) Xiong, T.; Cen, W. L.; Zhang, Y. X.; Dong, F. *ACS Catal.* **2016**, *6*, 2462−2472.
(27) Myung, N.; Bae, Y.; Bard, A. J. *Nano Lett.* **2003**, *3*, 1053−1055.
(28) Zanut, A.; Palomba, F.; Scota, M. R.; Rebeccani, S.; Marcaccio, M.; Genovese, D.; Rampazzo, E.; Valenti, G.; Paolucci, F.; Prodi, L. *Angew. Chem., Int. Ed.* **2020**, *59*, 21858−21863.
(29) Chen, A. Y.; Liang, W. B.; Wang, H. J.; Zhuo, Y.; Chai, Y. Q.; Yuan, R. *Anal. Chem.* **2020**, *92*, 1379−1385.
(30) Wang, F.; Liu, J.; Wang, H. Y.; Yu, S. S.; Cui, X. Q.; Ali, A.; Wu, T.; Liu, Y. *Nanoscale* **2018**, *10*, 15932−15937.